



## A fiber-shaped neural probe with alterable elastic moduli for direct implantation and stable electronic–brain interfaces†

Cite this: *J. Mater. Chem. B*, 2020, **8**, 4387

Received 25th February 2020,  
Accepted 20th April 2020

DOI: 10.1039/d0tb00508h

rsc.li/materials-b

Chengqiang Tang,<sup>a</sup> Songlin Xie,<sup>a</sup> Mengying Wang,<sup>a</sup> Jianyou Feng,<sup>a</sup> Zhengqi Han,<sup>b</sup> Xiaoying Wu,<sup>a</sup> Liyuan Wang,<sup>a</sup> Chuanrui Chen,<sup>a</sup> Jijia Wang,<sup>a</sup> Liping Jiang,<sup>a</sup> Peining Chen,<sup>a</sup> Xuemei Sun<sup>ib</sup>\*<sup>a</sup> and Huisheng Peng<sup>ib</sup><sup>a</sup>

Researchers developing implantable neural probes face a dilemma. Rigid neural probes facilitate direct implantation, but the brain tissue suffers from a vulnerable interface and a strong neuroinflammatory response due to mechanical mismatch between the probe and the brain tissue. Flexible neural probes offer stable interfaces and eliminate neuroinflammatory responses but require auxiliary implantation. Here, we have created a new kind of micro fiber-shaped neural probe with alterable elastic moduli before and after implantation. Carbon nanotube fibers and calcium crosslinked sodium alginate functioned as the core electrode and sheath layer, respectively. The response of calcium crosslinked sodium alginate to water will alter the probe elastic moduli from ~10 GPa to ~10 kPa post implantation, which is close to the elastic modulus of brain tissue. The micro fiber probes were directly implanted into mouse brains without any additional materials. After implantation, they became soft and offered dynamically adaptable interfaces with a reduced inflammatory response, benefiting long-term monitoring of neuron signals. Continuous four week monitoring of neuron signals was achieved. The simplicity of the strategy makes it suitable for versatile neuron techniques in neuron recording and modulation.

Neural recording technologies have contributed considerably to understanding brain and neural disorders by revealing neuron activities and functional connectivity.<sup>1–3</sup> Originating from tungsten (W)<sup>4</sup> and silicon probes, Michigan probes,<sup>5</sup> Utah arrays<sup>6</sup> and dense packing electrodes in Neuropixels probes<sup>7</sup> have enabled the advanced spatiotemporal and multi-functional interrogation of neurons. Their rigid nature enables direct implantation with minimized tissue damage and accurate localization in the brain. However, the interfaces established between rigid

probes and soft tissue are still not biologically and mechanically stable, *i.e.*, yielding tissue damage and eliciting a foreign body response that eventually blocks the interface through glial scarring especially during long-term monitoring<sup>8,9</sup> (Scheme 1). Instead, soft materials are increasingly used in neural interfaces to provide more stable interfaces while minimizing side effects.<sup>10,11</sup> However, implantation and localization of the soft material in soft tissues is challenging, alongside a lack of available tools to avoid rigid auxiliary materials that are associated with additional tissue damage, lengthy interface recovery and micromotion of the soft electrode.<sup>12–14</sup> The dilemma of choosing between simplified implantation and stable interfaces has called for the evolution of materials and fabrication techniques for neuronal recording technology.

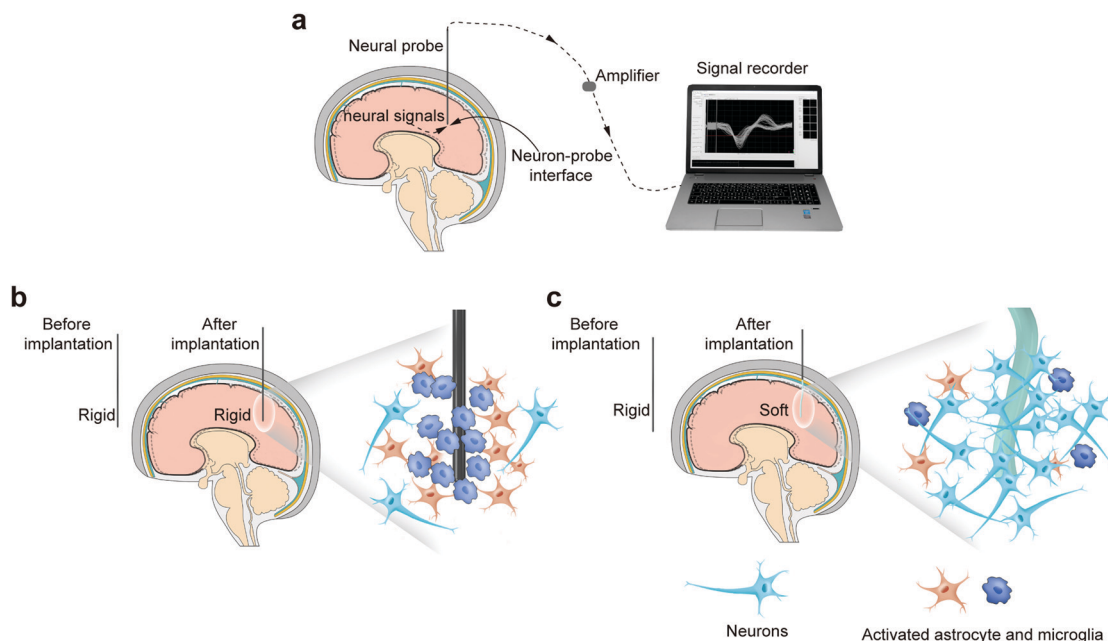
Material and machinery strategies have been attempted to implant soft neural probes into soft brain tissues, *e.g.*, surface coating<sup>15–17</sup> and fluidic microactuation.<sup>18</sup> Taking advantage of their gradient dissolution under physiological conditions, sucrose and polyethylene glycol have been used as surface layers to assist implantation. However, their dissolution was always associated with an increase in osmotic pressure, which influenced the biological activities of a large region of surrounding cells.<sup>19</sup> Machinery strategies like fluidic microactuation do not require the adoption of dissolvable compounds but the motions of soft electrodes and targeting to interested cells are far from controllable. Therefore, new strategies should be explored from both scientific and engineering aspects to meet the requirement of soft probes.

Here, we developed microfiber-shaped neural probes (MFNPs) with alterable elastic moduli, *i.e.*, as rigid as metal wires to ensure a facile and direct implantation and becoming as soft as brain tissue after implantation to ensure dynamic and stable interfaces (Scheme 1). The probe featured a coaxial structure, where carbon nanotube fiber (CNTF) served as the core electrode<sup>20</sup> and calcium ion crosslinked sodium alginate (SA) functioned as the shell.<sup>21</sup> The elastic modulus of dry-state MFNP (Dry-MFNP) was determined to be  $9.5 \pm 0.5$  GPa,  $10^6$  times to that of brain tissue ( $3.0 \pm 0.3$  kPa). Therefore, the implantation does not require the

<sup>a</sup> State Key Laboratory of Molecular Engineering of Polymers, Department of Macromolecular Science and Laboratory of Advanced Materials, Fudan University, Shanghai 200438, China. E-mail: sunxm@fudan.edu.cn

<sup>b</sup> School of Life Sciences, State Key Laboratory of Medical Neurobiology, Collaborative Innovation Center for Brain Science, Fudan University, Shanghai 200433, China

† Electronic supplementary information (ESI) available. See DOI: 10.1039/d0tb00508h



**Scheme 1** Neural probes with alterable elastic moduli. (a) Through the neuron–probe interface, neural signals are transmitted to a computer. (b) Rigid probes have the benefit of direct implantation, but the mechanical mismatch leads to a neuroinflammatory response with chronic use. (c) Alterable MFNP neural probes ensure direct implantation and become soft after implantation, with the benefit of a stable neuron–probe interface and a reduced neuro-inflammatory response.

additional assistance of a rigid metal wire which is associated with inevitable increased tissue damage or a sacrificial layer like sucrose, the dissolution of which will lead to a change of the surrounding environment and cell death. After implantation, the Dry-MFNP absorbed water and became soft with elastic moduli of  $7.9 \pm 3.1$  kPa, close to the values of brain tissue, and was named Wet-MFNP. The matched elastic modulus ensured a synchronized motion between Wet-MFNP and the brain tissue, thus providing a stable interface and finally delivering a highly stable neuron signal recording especially during long-term application. Furthermore, the inflammatory response triggered by the relative motion and injury was eliminated.

The typical preparation of an MFNP is illustrated in Fig. 1a. CNTFs were continuously produced and collected *via* floating catalyzed chemical vapor deposition, followed by a dry spinning process (Fig. S1, ESI<sup>†</sup>).<sup>22</sup> By adjusting the twisting speed, twisting time and the original diameter from the chemical vapor deposition, we could control the diameter of the CNTF from 20 to 100  $\mu\text{m}$ . A parylene insulating layer of about 2  $\mu\text{m}$  was coated onto the surface of the CNTF by vacuum vapor deposition to obtain the insulated CNTF<sup>23</sup> (I-CNTF, Fig. S2, ESI<sup>†</sup>). The I-CNTF was inserted into a silicone tube with a diameter of 300  $\mu\text{m}$  and then the tube was syringe-injected with 2 wt% SA solution. After completely filling, the silicone tube was stretched to 200% of its original length and was then immersed in liquid nitrogen. In liquid nitrogen, the environmental temperature was below the glass transition temperature of the silicone tube.<sup>24</sup> After lifting the tube out the liquid nitrogen, the length and diameter of the silicone tube recovered rapidly. When the SA was frozen, the fiber was easily released

from the silicone tube. The fiber was then transferred to aqueous  $\text{Ca}^{2+}$  solution for further crosslinking (Fig. S3, ESI<sup>†</sup>) for 1 h.<sup>25</sup> After drying at 80  $^{\circ}\text{C}$  for 1 h, an MFNP with a three-layer core–shell structure was obtained (Fig. 1b), where the CNTF, parylene and  $\text{Ca}^{2+}$  crosslinked SA served as the neural electrode, insulation layer and alterable layer, respectively (Fig. 1c).

Typically, the diameter of the CNTF was  $\sim 20$   $\mu\text{m}$  (Fig. 1c-i and Fig. S4, ESI<sup>†</sup>). After coating with parylene, the diameter was  $\sim 24$   $\mu\text{m}$  (Fig. 1c-ii). The Dry-MFNP had a diameter of  $\sim 36$   $\mu\text{m}$  and its surface was smooth (Fig. 1c-iii), which would mean a reduced resistance during the implanting process. The Dry-MFNP could be kept upright with only one end fixed (Fig. 1d) for a relatively high elastic modulus, while the Wet-MFNP was flexible enough to be bent, folded or wrapped into versatile shapes and in three dimensions (Fig. 1e and Fig. S5, ESI<sup>†</sup>). The microscope image of a Wet-MFNP revealed that the overall diameter of the Wet-MFNP was about 190  $\mu\text{m}$  in total with a  $\sim 83$   $\mu\text{m}$  SA shell (Fig. 1f). Indeed, the diffusion of water molecules and the relaxation of the polymer chains in the aqueous environment contributed to the swelling of SA, resulting in the corresponding alteration of the elastic modulus and flexibility.<sup>26</sup> We observed the internal structure of Dry-MFNP and Wet-MFNP after freeze drying, and the Wet-MFNP demonstrated a more porous structure in accordance with previous reports<sup>27</sup> (Fig. S6, ESI<sup>†</sup>). These data explain the highly reversible transition.

The implanting process of Dry-MFNP was then carefully studied with transparent agar hydrogels with artificial cerebrospinal fluid from mice as the solvent (as a substitute for a brain), because they showed similar mechanical properties and fluid

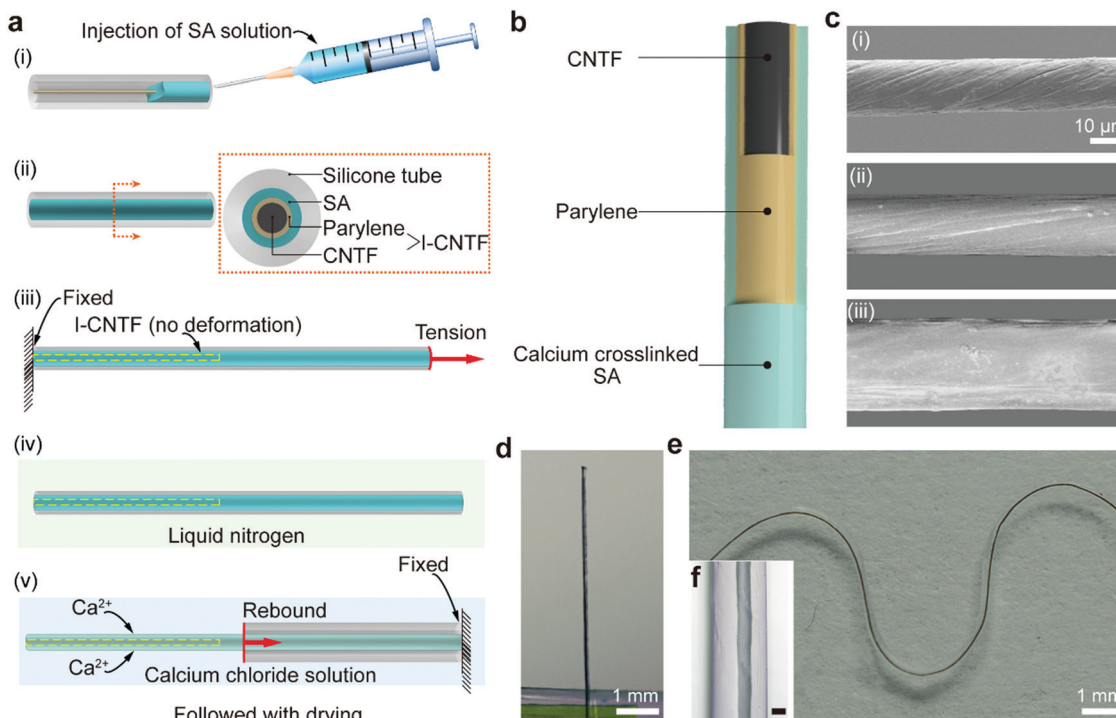


**Fig. 1** Preparation of the alterable MFNP. (a) The typical procedures to fabricate an MFNP. (i) A parylene-insulated carbon nanotube fiber (I-CNTF) was inserted into a silicone tube, followed by an injection of sodium alginate (SA) solution. (ii) A three-layer coaxial structure was obtained, *i.e.*, I-CNTF, SA and a silicone tube from the inside out. (iii) With one end fixed, the silicone tube and SA part were stretched to 200% of their original length. (iv) The fiber was immersed in liquid nitrogen. (v) The fiber was transferred to calcium chloride solution. With one end released, the silicone tube rebounded, and the exposed SA was crosslinked by  $\text{Ca}^{2+}$ . (b) Schematic of an MFNP with a layered structure. (c) Scanning electron microscope images of CNTF, I-CNTF and Dry-MFNP. (d) Photograph of a Dry-MFNP. (e) Photograph of a Wet-MFNP immersed in artificial brain cerebrospinal fluid (inset (f) photograph of a Wet-MFNP at high magnification, scale bar: 50  $\mu\text{m}$ ).

components. The Dry-MFNP was implanted into the agar hydrogel without any auxiliary materials and maintained for about 50 s before being pulled out. The fiber was intended to implant into the gel for the second time but it failed. The end of the fiber bent easily rather than remaining still, indicating that the MFNP had turned into a soft Wet-MFNP (Fig. 2a and Movie S1, ESI<sup>†</sup>). The MFNP without a hydrogel layer, *i.e.* I-CNTF, also bent and failed to penetrate into the gel due to the low elastic modulus (Movie S2, ESI<sup>†</sup>).

The bending forces were further tested for the Dry-MFNPs soaked in the artificial cerebrospinal fluid of mice for different periods of time. As the test curves showed, the bending force dropped from 0.04 to 0.02 N in 1 s, further dropped to 0.002 N at 10 s and then remained relatively stable (Fig. 2b and Fig. S7, ESI<sup>†</sup>). This indicated that the Dry-MFNP achieved elastic modulus conversion in a short period of time, and the implantation time utilized in the animal experiment should be controlled within 10 s.

The mechanical difference between Dry-MFNP and Wet-MFNP was then studied using the nanoindentation method. Gold (Au) wire<sup>28</sup> and brain tissue were also tested as rigid and soft materials under the same conditions, respectively. The nanoindentation curves of the Dry-MFNP and Wet-MFNP were far apart (Fig. 2c). Under the Hertzian contact model<sup>29</sup> fitting over several repeated test results, the effective indentation

elastic moduli ( $E_{\text{eff}}$ ) of the Dry-MFNPs were determined to be  $9.7 \pm 0.5$  GPa, close to those of Au wire ( $10.0 \pm 0.3$  GPa) (Fig. 2d and f). The  $E_{\text{eff}}$  of Wet-MFNPs were determined to be  $7.9 \pm 3.1$  kPa, close to those of brain tissue ( $3.0 \pm 0.3$  kPa) (Fig. 2e and f). The  $E_{\text{eff}}$  of Dry-MFNPs was  $10^6$  times to that of Wet-MFNPs, which ensured both direct implantation and a stable interface with brain tissue.

Factors related to the elastic modulus alteration, especially the weight content of  $\text{Ca}^{2+}$ , were then evaluated. MFNPs were kept in aqueous solution with gradient  $\text{Ca}^{2+}$  weight percentages for 1 hour. The mechanical properties (*i.e.*, the  $E_{\text{eff}}$ ) of both the Dry-MFNP and Wet-MFNP were studied (Fig. 2g) *via* the nanoindentation method. Along with the increasing weight content of  $\text{Ca}^{2+}$ , the  $E_{\text{eff}}$  of the Dry-MFNPs continuously decreased while the  $E_{\text{eff}}$  of the Wet-MFNPs continuously increased. The higher  $\text{Ca}^{2+}$  content provided a higher crosslinking speed of the SA especially on the surface. In addition, the crosslinked surface would further limit the diffusion of  $\text{Ca}^{2+}$  and crosslinking inside, resulting in fewer crosslinking junctions and lower elastic moduli in the dry state. When soaked in artificial cerebrospinal fluid, the diffusion of water molecules was more difficult, which in turn resulted in a higher elastic modulus in the wet state.<sup>30</sup> Thermal gravimetric analysis (TGA) results further confirmed the hypothesis (Fig. 2h). With the increasing  $\text{Ca}^{2+}$  content, the water content in the Wet-MFNPs decreased.

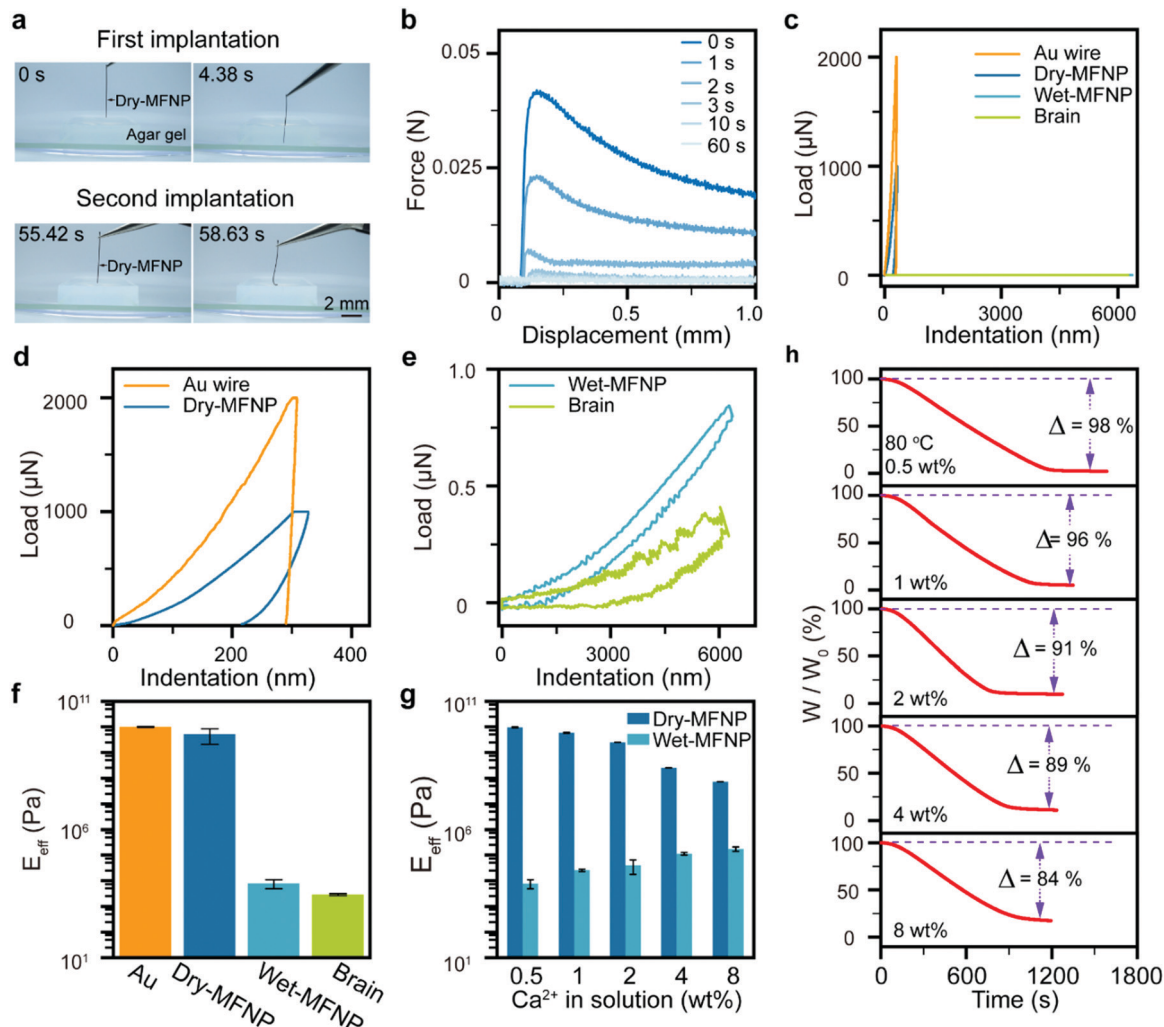


**Fig. 2** Alterable mechanical properties of the MFNP. (a) First and second implantation of the MFNP in agar gel. (b) Bending forces of the MFNP after immersion in artificial mice brain cerebrospinal fluid for different lengths of time. (c) Mechanical properties of Dry-MFNP, Wet-MFNP, gold (Au) wire and mouse brain tissue by the nanoindentation method. (d) Magnified mechanical curves of Dry-MFNP and Au wire in (c). (e) Magnified mechanical curves of the Wet-MFNP and mouse brain tissue in (c). (f) Effective indentation elastic moduli of Au wire, Dry-MFNP, Wet-MFNP and mouse brain tissue ( $n = 3$ ). (g) Effective indentation elastic modulus change of MFNPs crosslinked in aqueous solution with different weight percentages of  $\text{Ca}^{2+}$ . (h) Thermal gravimetric analysis (TGA) curves of Wet-MFNPs crosslinked in aqueous solution with different weight percentages of  $\text{Ca}^{2+}$ .

In other words, the diffusion of water molecules was limited. This was consistent with the elastic modulus regulation. For a direct implantation and a stable interface, the MFNPs used in this article were crosslinked in 0.5 wt%  $\text{Ca}^{2+}$  solution.

These fibers were then implanted into agar gels to study the interface between these two parts (Fig. 3a). The penetration depth was set at 5 mm, 0.6 wt% agar gel was used to simulate the situation of a brain.<sup>31</sup> As the state-of-the-art neural electrodes shared a high elastic modulus, *i.e.* hundreds of GPa (Table S1, ESI<sup>†</sup>), they thus contributed to a similar interface post implantation. Here, the commercial W wire for the electrophysiological recording was selected as a representative rigid electrode to compare with the Wet-MFNPs. For the MFNPs, the calcium-crosslinked SA in the dehydrated state in the Dry-MFNP began to swell, became soft, and finally occupied the space and formed a stable interface after implantation. The pull-out

forces were tested to infer the interface stability (Fig. 3b). The pull-out force increased from 1.7 to 4.6 mN with increasing the holding time from 0 to 60 s. For the W wire, the force curves before and after implantation for 60 s almost overlapped with a peak force of only 0.4 mN, much lower than that of the MFNP.

Considering the tissue dynamics, *e.g.*, the heart endures 1 000 000 times of repeated 20% volume expansion in one day,<sup>32,33</sup> we further studied the dynamic stability of the interface. A stable dynamic interface firstly called for a matched bending stiffness.<sup>34</sup> We used a dynamic mechanical analyzer in a single-cantilever mode to quantify the stiffness of fibers with a length of 5 mm in the frequency range of mammalian locomotion, *e.g.*, respiration and heartbeat (0.01–10 Hz). During the dynamic mechanical test, the Wet-MFNPs remained stable over the frequency range and demonstrated stiffness values of 43–60  $\text{N m}^{-1}$ , much lower than those of the W wires

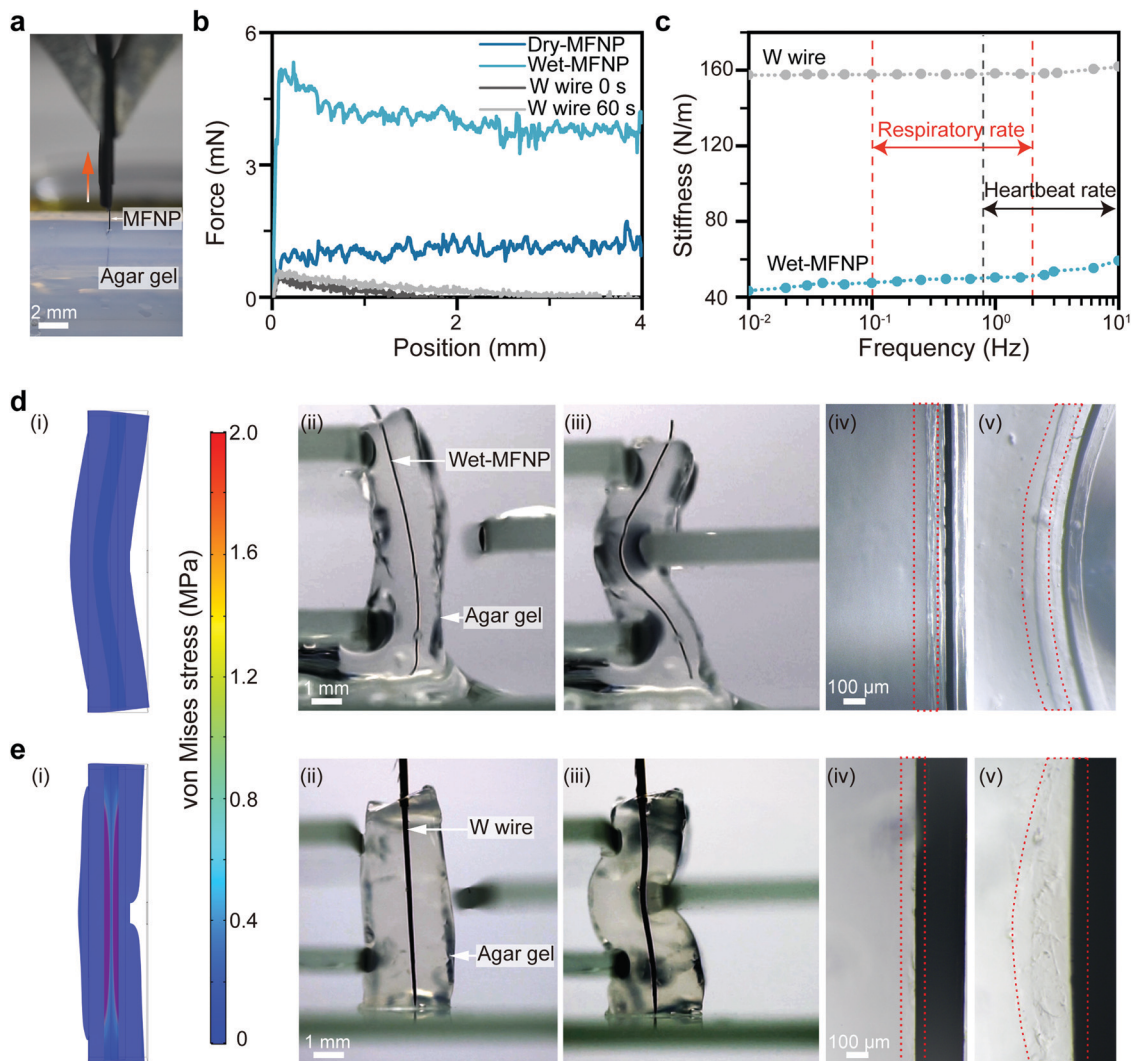


**Fig. 3** A dynamic stable interface between the MFNP and soft gel. (a) Photograph of the interface adhesion force test setup. (b) Adhesion forces of the MFNP and commercial tungsten (W) wire before and after being kept in agar gel for 60 s. (c) The measured bending stiffness of W wires and Wet-MFNPs at different frequencies with respiration and heartbeat rates covered in the testing range. The displacement amplitude was set as 50  $\mu\text{m}$ . (d) and (e) Bending performance of Wet-MFNPs and W wires with soft gels, respectively. (i) Simulated stress distribution of the Wet-MFNP and W wire implanted medium with a stick pressed to achieve the same deformation of the middle part using the finite element analysis method. (ii) and (iii) Photographs of the gels implanted with Wet-MFNP and W wire before and after a stick was pressed to their middle part, respectively. (iv) and (v) Optical micrographs of the probe–soft gel interface before and after bending, respectively.

(160–198  $\text{N m}^{-1}$ , Fig. 3c) and Dry-MFNPs (100–120  $\text{N m}^{-1}$ , Fig. S8, ESI $^\dagger$ ). The elasticity of the Wet-MFNPs was also improved to match nerves, *i.e.*, stress and strain of 10 MPa and 25%, respectively<sup>9</sup> (Fig. S9 and S10, ESI $^\dagger$ ).

Finite element analysis was then utilized to reveal the interfacial stress distribution during motion (Fig. 3d–i, e–i and Fig. S11, ESI $^\dagger$ ). In the simulation model, the elastic moduli of the medium and fibers were set to equal those of brain tissue and Wet MFNPs or W wires, respectively. After implanting the probes, the two ends of the medium were fixed, and a stick was utilized to press the middle part of the medium to reach the same deformation. The simulation did not involve the influence of gravity. Heavy stress concentration occurred at the interface, and a maximal stress of 0.84 MPa was found in

the W wire group. The interfacial stress at the Wet-MFNP/medium group was distributed evenly and was only 0.50 kPa, close to the surrounding medium (Fig. S12, ESI $^\dagger$ ).

To verify the simulation, 0.6 wt% agar gels were implanted with MFNPs and commercial W wires, and the interfaces were carefully observed. Three glass slides were used as sticks and placed on the top, middle and bottom parts of the fiber implanted gels, respectively (Fig. 3d–ii–iii, e–ii–iii and Movie S3, ESI $^\dagger$ ). When the gels were pressed by the middle glass slide, the deformation of the Wet MFNP and W wire were significantly different, *i.e.*, the Wet-MFNP bent with the gels while the W wire kept still. Detailed information at the interface before and after the deformation was collected with a microscope. For the Wet-MFNP/agar gel, the interface was neat, clear

and stable during the pression (Fig. 3d-iv-v). As for the W wire/agar gel, the interface was similar to the Wet-MFNP/agar gel interface before pressing, but it then broke after pressing for the W wire and failed to deform with the agar gel (Fig. 3d-iv-v). The W wire and gel were clearly separated. The interface separation displayed a crescent-shaped damage zone consistent with the

simulation results. The interfaces between the MFNP and soft gel also remained stable throughout the bending cycles at a frequency of 1 Hz (Fig. S13, ESI†). After 1000 cycles, the ratio of the distance change between the MFNP and the gel was only 1%.

The dynamic interface was further verified in a mouse brain. A 5 mm-long Dry-MFNP was implanted, and compression was

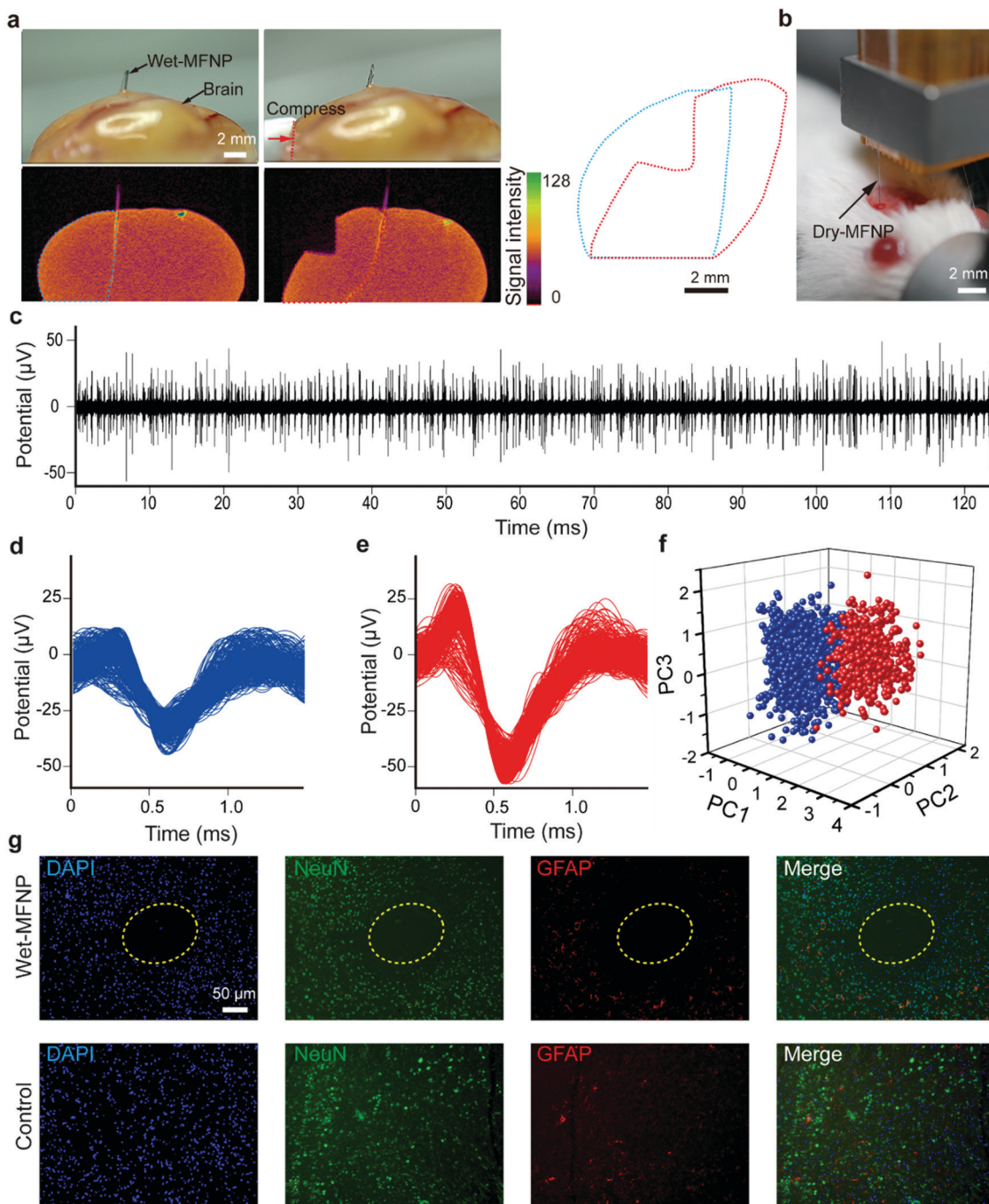


Fig. 4 Electrophysiological application of the MFNP *in vivo*. (a) Photographs (top) and micro-CT images (bottom) of a mice brain implanted with an MFNP before and after compression. The right image is the contour extraction line. (b) Photograph of implantation of an MFNP into a mouse brain. (c) A fragment of endogenous activity with MFNP as the neuronal probe. (d) and (e) Action-potential of the two units in (c). (f) Principal-component analysis (PCA) of the two neuronal units in (c). (g) Immunohistochemical images stained with neuron and astrocyte markers of brain slices implanted with (top) and without (bottom) MFNP for one week. Blue, DAPI, nucleus; green, NeuN, neurons; red, GFAP, astrocytes. The yellow dotted circles indicate the position of the MFNP.

applied on the top left side of the brain. Micro-CT images were collected to reveal the motions of the Wet-MFNP in the brain. The Wet-MFNP bent along with the compression and the extracted contour lines showed a synchronized motion of the fiber with the compressed brain (Fig. 4a).

A Dry-MFNP with a sharpened tip was implanted in the cerebral cortex of isoflurane anesthetized adult mice with the help of a micro pusher (Fig. 4b) to monitor the real-time neuronal activities. Before implantation, the impedance and volt-ampere characteristics of the Wet-MFNP were tested using an electrochemical workstation. For the Wet-MFNP, as shown in Fig. S14 and S15 (ESI<sup>†</sup>), the impedance at 1 kHz was lower and the charge injection capacity was higher than the W wire. Then the probes were implanted in the mice brain with a depth of 2 mm.<sup>35</sup> Fig. 4c showed 125 s excerpts obtained from the active probe after 600–3000 Hz band pass filtering. Since the sizes of the conductive CNTF and the neuron were on the same scale, the Wet-MFNP might be capable of recording signals of a single unit. Two single unit waveforms were demonstrated in Fig. 4d and e, and principal components analysis (PCA) of the spike waveforms revealed two neuronal units with good cluster-separation quality (Fig. 4f). The two single units had peak-to-peak voltages of 39.7 and 41.9  $\mu\text{V}$ , and signal to noise ratios (SNRs) of 5.93 and 8.16 (real-time values determined by the software CerePlexDirect of Blackrock), respectively. The SNR of MFNP outperformed most flexible neural probes based on polymer materials.<sup>36</sup> The I-CNTF without a hydrogel layer was also implanted into the brain to record the neural activity (Fig. S16, ESI<sup>†</sup>). The SNR of I-CNTF was determined to be 5.50, which was close to that of MFNP. This means that the hydrogel did not reduce signal quality. It has been reported that the soft sheath could protect neuron cells from mechanical damage.<sup>37,38</sup>

For long-term recording, the swelling properties and stability of sodium alginate hydrogel was further clarified. After soaking in artificial cerebrospinal fluid for 25 minutes, the diameter of the MFNP was well maintained and no obvious increase was observed (Fig. S17, ESI<sup>†</sup>). We further used the change of mass ratio before and after soaking in artificial cerebrospinal fluid for different periods of time to study the stability of calcium ion-crosslinked sodium alginate. It was found that the ratio remained stable during a long soaking duration of one week (Fig. S18, ESI<sup>†</sup>).

Then, neural recording was conducted for 4 weeks, and no obvious performance degradation was found (Fig. S19, ESI<sup>†</sup>). This stability might come from the stable electrochemical performance of the probes and the limited inflammatory response ensured by the dynamic stable interface. The result of the long-term testing *in vitro* showed that the impedance of the Wet-MFNP remained in a stable state for four weeks (Fig. S20, ESI<sup>†</sup>). The inflammatory response triggered by the MFNP was another factor related to the recording stability. According to the previous reports, the intensity of the inflammatory response tends to decrease 1 week post implantation.<sup>34,39</sup> Given this fact, the inflammatory response at the 7th day was determined, where the hexaribonucleotide binding protein-3 (NeuN) was used to mark neurons, glia fibrillary acidic protein (GFAP) was used to mark

astrocytes, and ionized calcium-binding adaptor molecule 1 (Iba1) was used to mark gliocytes.<sup>40</sup> As shown in Fig. 4g and Fig. S21 (ESI<sup>†</sup>), negligible neuronal cell loss and glial response were induced by a Wet-MFNP, which lays a solid foundation for future *in vivo* application from a biological point of view.

To summarize, we presented a type of micro fiber-shaped neuron probe with alterable elastic moduli, *i.e.*, as rigid as a metal wire which enabled direct implantation and as soft as brain tissue to deliver a biologically and mechanically stable interface. This technique mainly takes advantage of the smart elastic modulus conversion of crosslinked sodium alginate in response to water. The probes endured synchronized motion with soft gels/tissues under dynamic mechanical analysis and delivered a stable neuron recoding over four weeks *in vivo*. Besides carbon nanotube fibers for electrical signalling, this probe structure can be further engineered readily with advanced spatial or multi-functional integration. Thus, this approach holds great potential in application in versatile neuronal interfaces including but not restricted to neuronal interrogation, modulation and therapeutic intervention.

## Author contributions

X. S., S. X. and C. T. conceived the idea and designed the experiment. C. T. and M. W. fabricated the probes. C. T. performed the *in vitro* experiments. C. T., J. F., Z. H., X. W., L. W. and J. W. performed the *in vivo* experiments. L. J. performed the Micro-CT. All the authors participated in analyzing the data and preparing the manuscript.

## Conflicts of interest

There are no conflicts of interest to declare.

## Acknowledgements

This work was supported by the NSFC (21634003, 51673043 and 21805044), MOST (2016YFA0203302), STCSM (17QA1400400 and 19QA1400800), SHMEC (2017-01-07-00-07-E00062) and the Yanchang Petroleum Group.

## Notes and references

- 1 G. Hong and C. M. Lieber, *Nat. Rev. Neurosci.*, 2019, **20**, 330–345.
- 2 J. A. Frank, M. J. Antonini and P. Anikeeva, *Nat. Biotechnol.*, 2019, **37**, 1013–1023.
- 3 T. D. Yoshida Kozai, N. B. Langhals, P. R. Patel, X. Deng, H. Zhang, K. L. Smith, J. Lahann, N. A. Kotov and D. R. Kipke, *Nat. Mater.*, 2012, **11**, 1065–1073.
- 4 D. H. Hubel, *Science*, 1957, **125**, 549–550.
- 5 K. D. Wise, J. B. Angell and A. Starr, *IEEE Trans. Biomed. Eng.*, 1970, **BME-17**, 238–247.
- 6 P. K. Campbell, K. E. Jones and R. A. Normann, *Biomed. Sci. Instrum.*, 1990, **26**, 161–165.

- 7 J. J. Jun, N. A. Steinmetz, J. H. Siegle, D. J. Denman, M. Bauza, B. Barbarits, A. K. Lee, C. A. Anastassiou, A. Andrei, Ç. Aydin, M. Barbic, T. J. Blanche, V. Bonin, J. Couto, B. Dutta, S. L. Gratiy, D. A. Gutnisky, M. Häusser, B. Karsh, P. Ledochowitsch, C. M. Lopez, C. Mitelut, S. Musa, M. Okun, M. Pachitariu, J. Putzeys, P. D. Rich, C. Rossant, W. L. Sun, K. Svoboda, M. Carandini, K. D. Harris, C. Koch, J. O'Keefe and T. D. Harris, *Nature*, 2017, **551**, 232–236.
- 8 J. K. Nguyen, D. J. Park, J. L. Skousen, A. E. Hess-Dunning, D. J. Tyler, S. J. Rowan, C. Weder and J. R. Capadona, *J. Neural Eng.*, 2014, **11**, 056014.
- 9 S. P. Lacour, G. Courtine and J. Guck, *Nat. Rev. Mater.*, 2016, **1**, 16063.
- 10 M. Lee, H. J. Shim, C. Choi and D. H. Kim, *Nano Lett.*, 2019, **19**, 2741–2749.
- 11 J. Goding, C. Vallejo-Giraldo, O. Syed and R. Green, *J. Mater. Chem. B*, 2019, **7**, 1625–1636.
- 12 Z. J. Du, C. L. Kolarcik, T. D. Y. Kozai, S. D. Luebben, S. A. Sapp, X. S. Zheng, J. A. Nabity and X. T. Cui, *Acta Biomater.*, 2017, **53**, 46–58.
- 13 T. Il Kim, J. G. McCall, Y. H. Jung, X. Huang, E. R. Siuda, Y. Li, J. Song, Y. M. Song, H. A. Pao, R. H. Kim, C. Lu, S. D. Lee, I. S. Song, G. Shin, R. Al-Hasani, S. Kim, M. P. Tan, Y. Huang, F. G. Omenetto, J. A. Rogers and M. R. Bruchas, *Science*, 2013, **340**, 211–216.
- 14 L. Lu, X. Fu, Y. Liew, Y. Zhang, S. Zhao, Z. Xu, J. Zhao, D. Li, Q. Li, G. B. Stanley and X. Duan, *Nano Lett.*, 2019, **19**, 1577–1586.
- 15 T. D. Y. Kozai, Z. Gugel, X. Li, P. J. Gilgunn, R. Khilwani, O. B. Ozdoganlar, G. K. Fedder, D. J. Weber and X. T. Cui, *Biomaterials*, 2014, **35**, 9255–9268.
- 16 N. V. Apollo, J. Jiang, W. Cheung, S. Baquier, A. Lai, A. Mirebedini, J. Foroughi, G. G. Wallace, M. N. Shivdasani, S. Praver, S. Chen, R. Williams, M. J. Cook, D. A. X. Nayagam and D. J. Garrett, *Adv. Biosyst.*, 2018, **2**, 1700187.
- 17 S. Guan, J. Wang, X. Gu, Y. Zhao, R. Hou, H. Fan, L. Zou, L. Gao, M. Du, C. Li and Y. Fang, *Sci. Adv.*, 2019, **5**, aav2842.
- 18 F. Vitale, D. G. Vercosa, A. V. Rodriguez, S. S. Pamulapati, F. Seibt, E. Lewis, J. S. Yan, K. Badhiwala, M. Adnan, G. Royer-Carfagni, M. Beierlein, C. Kemere, M. Pasquali and J. T. Robinson, *Nano Lett.*, 2018, **18**, 326–335.
- 19 D. Wentz and K. Schügerl, *Enzyme Microb. Technol.*, 1992, **14**, 68–75.
- 20 R. Wieduwild, S. Krishnan, K. Chwalek, A. Boden, M. Nowak, D. Drechsel, C. Werner and Y. Zhang, *Angew. Chem., Int. Ed.*, 2015, **127**, 4034–4038.
- 21 Y. Cheng, K. H. Chan, X. Q. Wang, T. Ding, T. Li, X. Lu and G. W. Ho, *ACS Nano*, 2019, **13**, 13176–13184.
- 22 H. Peng, M. Jain, D. E. Peterson, Y. Zhu and Q. Jia, *Small*, 2008, **4**, 1964–1967.
- 23 L. Zhang, J. Yang, X. Wang, B. Zhao and G. Zheng, *Nanoscale Res. Lett.*, 2014, **9**, 448–455.
- 24 P. R. Dvornic and R. W. Lenz, *Macromolecules*, 1992, **25**, 3769–3778.
- 25 J. Y. Sun, X. Zhao, W. R. K. Illeperuma, O. Chaudhuri, K. H. Oh, D. J. Mooney, J. J. Vlassak and Z. Suo, *Nature*, 2012, **489**, 133–136.
- 26 B. D. Johnson, D. J. Beebe and W. C. Crone, *Mater. Sci. Eng., C*, 2004, **24**, 575–581.
- 27 K. Zhang, Y. Fang, Y. He, H. Yin, X. Guan, Y. Pu, B. Zhou, W. Yue, W. Ren, D. Du, H. Li, C. Liu, L. Sun, Y. Chen and H. Xu, *Nat. Commun.*, 2019, **10**, 53850–53866.
- 28 N. Xue, D. Wang, C. Liu, Z. Ke, P. Elia, T. Li, C. Chi, Y. Cheng and J. Sun, *Sens. Actuators, B*, 2018, **272**, 314–323.
- 29 J. L. Hay and P. J. Wolff, *J. Mater. Res.*, 2001, **16**, 1280–1286.
- 30 P. Aslani and R. A. Kennedy, *J. Controlled Release*, 1996, **42**, 75–82.
- 31 Z. J. Chen, G. T. Gillies, W. C. Broaddus, S. S. Prabhu, H. Fillmore, R. M. Mitchell, F. D. Corwin and P. P. Fatouros, *J. Neurosurg.*, 2004, **101**, 314–322.
- 32 P. C. Ivanov, L. A. N. Amaral, A. L. Goldberger, S. Havlin, M. B. Rosenblum, Z. Struzik and H. E. Stanley, *Nature*, 1999, **399**, 461–465.
- 33 V. Järvinen, M. Kupari, P. Hekali and V. P. Poutanen, *Am. J. Cardiol.*, 1994, **73**, 1135–1138.
- 34 A. Canales, X. Jia, U. P. Frieriep, R. A. Koppes, C. M. Tringides, J. Selvidge, C. Lu, C. Hou, L. Wei, Y. Fink and P. Anikeeva, *Nat. Biotechnol.*, 2015, **33**, 277–284.
- 35 K. Wang, C. L. Frewin, D. Esrafilzadeh, C. Yu, C. Wang, J. J. Pancrazio, M. Romero-Ortega, R. Jalili and G. Wallace, *Adv. Mater.*, 2019, **31**, 1805867.
- 36 S. Park, Y. Guo, X. Jia, H. K. Choe, B. Grena, J. Kang, J. Park, C. Lu, A. Canales, R. Chen, Y. S. Yim, G. B. Choi, Y. Fink and P. Anikeeva, *Nat. Neurosci.*, 2017, **20**, 612–619.
- 37 Y. Liu, A. F. Mcguire, H. Lou, T. L. Li, J. B. Tok, B. Cui and Z. Bao, *Proc. Natl. Acad. Sci. U. S. A.*, 2018, **115**, 11718–11723.
- 38 P. Cai, M. Layani, W. R. Leow, S. Amini, Z. Liu, D. Qi, B. Hu, Y. Wu, A. Miserez, S. Magdassi and X. Chen, *Adv. Mater.*, 2016, **28**, 3102–3110.
- 39 A. J. Williams, H. H. Wei, J. R. Dave and F. C. Tortella, *J. Neuroinflammation*, 2007, **4**, 17.
- 40 D. Ito, Y. Imai, K. Ohsawa, K. Nakajima, Y. Fukuuchi and S. Kohsaka, *Mol. Brain Res.*, 1998, **57**, 1–9.